



OPEN

SUBJECT AREAS:

ELECTRONIC PROPERTIES
AND MATERIALS

POLYMERS

CARBON NANOTUBES AND
FULLERENES

COMPOSITES

Received
30 July 2013Accepted
13 January 2014Published
28 January 2014Correspondence and
requests for materials
should be addressed to
K.H. (kenji-hata@aist.
go.jp)

Controlling exfoliation in order to minimize damage during dispersion of long SWCNTs for advanced composites

Howon Yoon¹, Motoi Yamashita¹, Seisuke Ata^{1,2}, Don N. Futaba^{1,2}, Takeo Yamada^{1,2} & Kenji Hata^{1,2}¹Technology Research Association for Single Wall Carbon Nanotubes (TASC), 1-1-1 Higashi, Tsukuba, Ibaraki 305-8565, Japan, ²Nanotube Research Center, National Institute of Advanced Industrial Science and Technology (AIST), 1-1-1 Higashi, Tsukuba, Ibaraki 305-8565, Japan.

We propose an approach to disperse long single-wall carbon nanotubes (SWCNTs) in a manner that is most suitable for the fabrication of high-performance composites. We compare three general classes of dispersion mechanisms, which encompass 11 different dispersion methods, and we have dispersed long SWCNTs, short multi-wall carbon nanotubes, and short SWCNTs in order to understand the most appropriate dispersion methods for the different types of CNTs. From this study, we have found that the turbulent flow methods, as represented by the Nanomizer and high-pressure jet mill methods, produced unique and superior dispersibility of long SWCNTs, which was advantageous for the fabrication of highly conductive composites. The results were interpreted to imply that the biaxial shearing force caused an exfoliation effect to disperse the long SWCNTs homogeneously while suppressing damage. A conceptual model was developed to explain this dispersion mechanism, which is important for future work on advanced CNT composites.

The superior mechanical, electrical, and thermal properties of carbon nanotubes (CNTs) and their high aspect ratios make them an attractive filler for composites. Following the first report on the preparation of composites using CNTs as a filler in 1994¹, the outstanding properties of CNTs have been utilized to develop multifunctional composites for applications in the fields of heat resistance, chemical sensing, electrical and thermal management, photoemission, electromagnetic absorption, energy storage performance, etc²⁻⁶. Although the potential of CNTs is well-recognized, it is not easy to disperse them while maintaining the intrinsic properties of the pristine CNTs^{7,8}. This is because CNTs can be regarded as macromolecules that have low solubility in organic solutions; as a result of the smooth surfaces of the CNTs, they have a strong tendency to bundle together through van der Waals interactions. Even for short CNTs, dispersion has been recognized as a serious problem, and these difficulties increase greatly as the length becomes longer or the aspect ratio becomes larger. Despite this difficulty, CNTs with higher aspect ratios are advantageous for accessing the full potential of CNTs in composites.

Recently, the advance of CNT synthesis has made it possible to grow of millimeter-scale CNTs⁹⁻¹², that are significantly longer than commercial single-wall carbon nanotubes (SWCNTs) and multi-wall carbon nanotubes (MWCNTs), which have lengths of ~10 μm. In particular, millimeter-scale SWCNTs can be grown, for example, by water-assisted chemical vapor deposition (CVD) as a vertically aligned CNT forest on a substrate¹². These forests can be produced on the kilogram-scale now, by continuously feeding the substrates into a CVD furnace using a belt conveyor^{13,14}. At present, these millimeter-scale SWCNTs are the conductive filler with the highest aspect ratio that can be utilized industrially. From a practical standpoint, increasing the SWCNT length has proven to be useful for realizing many composites exhibiting revolutionary but rational performance. For example, these long SWCNTs resemble long polymeric rubber chain molecules, and as such, when blended with polymers, they make a conductive composite that shows a high conductivity greater than 30 S/cm (>500 times that of a carbon black composite)¹⁵. Moreover, when stretched, the long SWCNTs deform in concert with the polymeric rubber chains to minimize the stress accumulation at the interfaces. In this way, the composites show excellent mechanical durability far exceeding that of existing conductive rubbers. As has been demonstrated, we envision that long SWCNTs could open up many new opportunities in the field of composites¹⁶, given sufficient advances in the dispersion technique and in the understanding of the dispersion mechanism to address to the fundamental requirements described above.

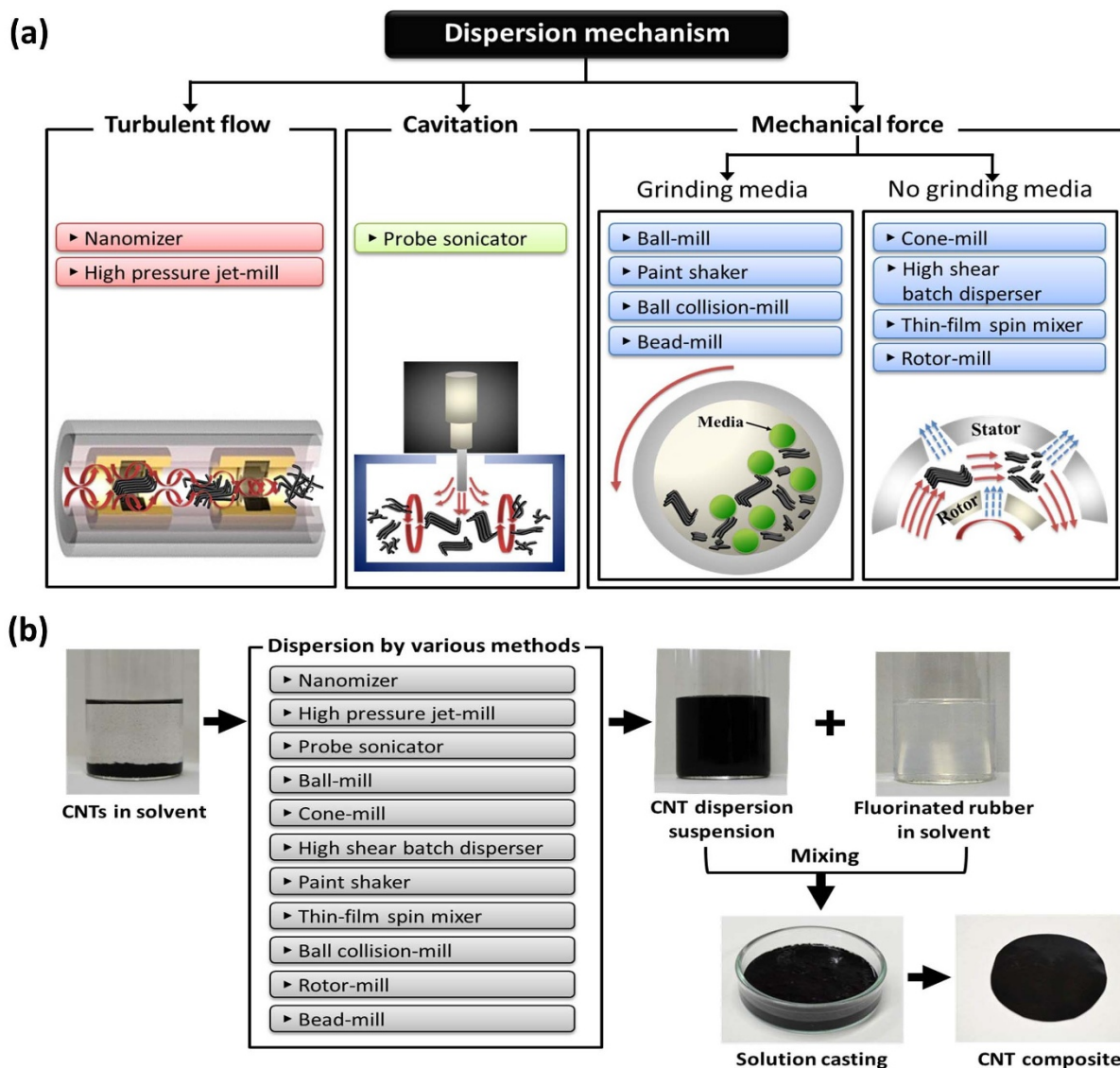


Figure 1 | Schematic of methods for dispersing nanotubes in rubbers. (a) Various dispersion methods for CNT classified into three general mechanisms: turbulent flow, cavitation, and mechanical force. (b) Process for CNT/rubber composite fabrication.

Over the past decade, CNT dispersion has been recognized as one of the key processes in composite fabrication, and therefore, numerous dispersion methods have been studied^{17–19}. For example, the most well-known method is ultrasonication, which is most commonly used to create a dispersion of isolated CNTs^{20–22}. Ball/bead milling is another conventional dispersion method, in which materials are ground by balls or beads into fine powders. Every dispersion method has its advantages, but also has its problems, and no method is ideal. We would like to point out that almost all previous dispersion studies have employed only one or two dispersion methods. To date, there has been no systematic study investigating the comparative performance of the different dispersion methods.

In this letter, we address these issues and propose a fundamental dispersion strategy that enables the potential of long SWCNTs to be applied to advanced composites. From a practical standpoint, we focus primarily on the comparison of many types of dispersion methods without the use of a surfactant, as an approach for exploring the appropriate method for dispersion of long SWCNTs. By comparing types of dispersion methods for long SWCNTs and three other commercially available shorter MWCNTs, we reveal that turbulent flow dispersion is the most effective and unique dispersion method as a result of its efficient and unique exfoliation of long

SWCNTs through the biaxial shearing force. We propose a model describing the dispersion effect as an interplay between the level of exfoliation and the level of damage introduced to the SWCNTs. We believe that this dispersion strategy should provide guidelines for the fabrication of advanced CNT composites.

Results

In this work, we attempted to clarify the best method of dispersing long SWCNTs and to understand the underlying mechanism. To achieve these goals, we selected 11 different methods that encompass three general kinds of dispersion mechanisms: turbulent flow, cavitation, and mechanical force (Fig. 1a). Specifically, the 11 dispersion methods studied in this work involve the use of the Nanomizer, high-pressure jet mill, probe sonicator, ball mill, bead mill, paint shaker, ball collision mill, cone mill, rotor mill, high-shear batch disperser, and thin-film spin mixer. The Nanomizer and the high-pressure jet mill disperse the CNTs using a turbulent flow. The probe sonicator disperses the CNTs through cavitation. The remaining methods use mechanical forces with or without the presence of grinding media (balls or beads). The methods with grinding media include ball milling, bead milling, the paint shaker method, and ball collision milling. Methods without grinding media are cone milling, rotor

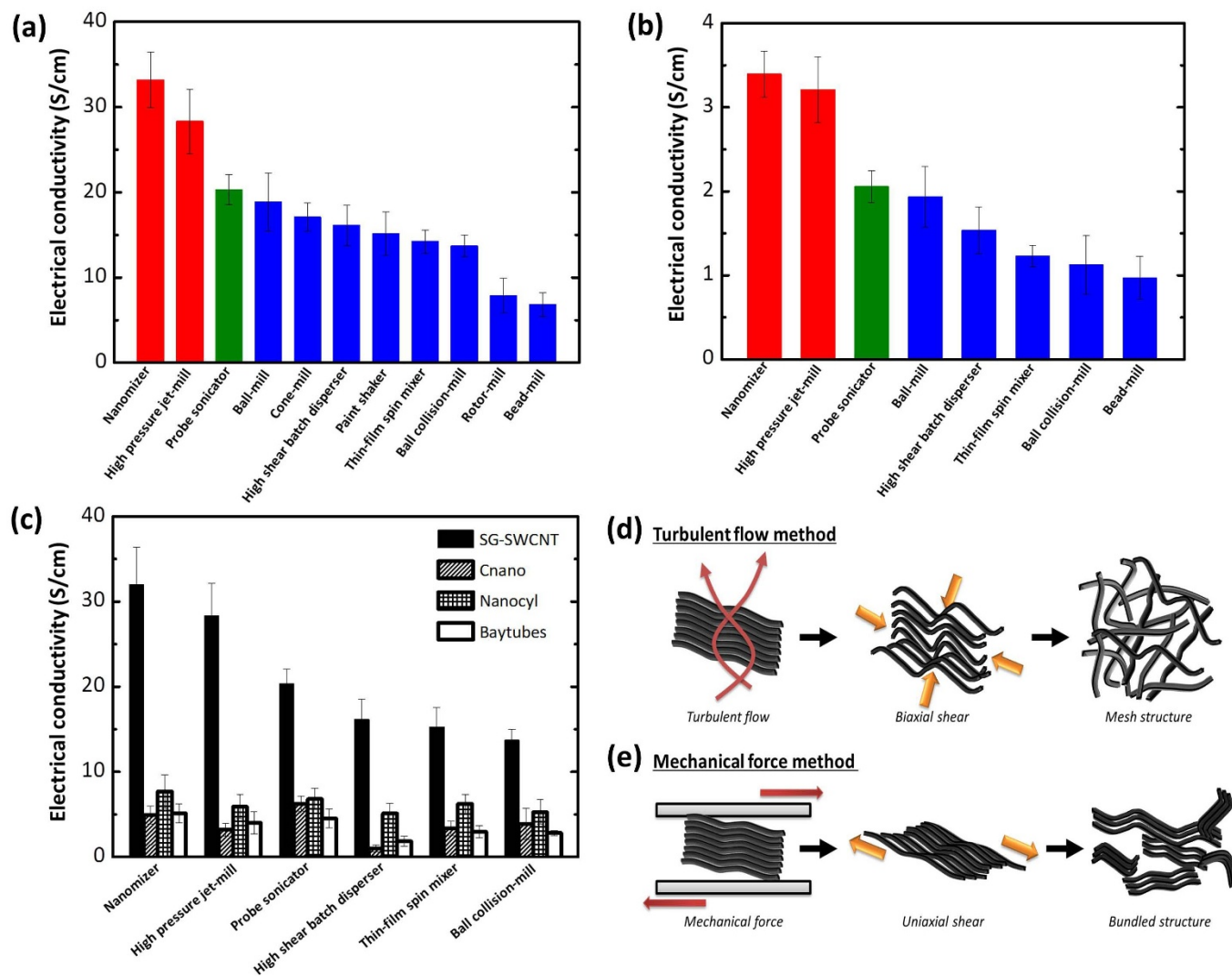


Figure 2 | Difference in electrical conductivity for CNT composites prepared using different dispersion methods. Electrical conductivity of (a) 10 wt% SG-SWCNT/fluorinated rubber composites and (b) 10 wt% SG-SWCNT/PS composites. Red bars: dispersed using turbulent flow methods. Green bar: dispersed using a cavitation method. Blue bars: dispersed using mechanical force methods. (c) Comparison of electrical conductivities of 10 wt% CNT/fluorinated rubber composites containing other MWCNTs (CNano, Nanocyl and Baytubes). (d, e) Model of the changes in the SG-SWCNT structures for two different dispersion mechanisms: (d) turbulent flow and (e) mechanical force.

milling, the high-shear batch disperser method, and the thin-film spin mixer method. With these 11 methods, we investigated the dispersion of long SWCNTs with minimum damage to fabricate composites (SWCNT rubbers) with superior performance (electrical conductivity).

Long SWCNTs were synthesized using the water-assisted CVD method, referred to as the “super-growth (SG) method,” to grow millimeter-scale-length (from 500 to 1,000 μm) SWCNT forests¹². To our knowledge, these are the longest CNTs with the highest aspect ratio that can be produced on the industrial scale. SWCNTs grown using the SG method are known to be very pure, with a carbon purity of 99.98% (carbon purity: mass of carbon content/total mass of sample $\times 100$), and a small average diameter (~ 3 nm), and thus the aspect ratio exceeds 10^6 . The intrinsic band gap of the semiconducting SG-SWCNTs is exceptionally small (~ 0.26 eV) and more similar to semi-metals. As such, we do not expect the chiral distribution of the SG-SWCNT samples to play a significant role in the conductivity properties. Therefore, these SG-SWCNTs have been proven to be useful in advanced composites, as described in the introduction.

We dispersed SG-SWCNT forests in methyl isobutyl ketone (MIBK) using the 11 dispersion methods and mixed them with a

fluorinated rubber to fabricate 10 wt% SG-SWCNT conducting rubber composites, as schematically shown in Fig. 1b. To verify the effect of the CNT dispersion method on the performance of the composites, we fixed the solution. We chose MIBK because it is known that the solubility parameter of MIBK matches with that of the SG-SWCNTs, and therefore the CNTs have a high solubility. In addition, MIBK has previously been chosen as a solution for dispersing CNTs into elastomers^{23,24}. We selected an elastomer composite as a representative composite, since it is well-recognized that long SWCNTs are crucial for highly conductive rubbers^{15,25}, and highly conductive rubbers are one of the key materials for the emerging field of stretchable electronics^{23,24}. Each of the 11 dispersion methods was optimized for the electrical conductivity of the composite by tuning only the dispersion time and strength. No surfactant was used in this study for the following reasons. First, when surfactants are used, the performance of the composite is affected by the surfactant-removal process, which is out of the scope of this paper. Second, from a practical and industrial standpoint, it is preferred not to use surfactants to simplify the fabrication process. The SG-SWCNT elastomer composites were obtained using solution casting. The solvent for the CNT dispersions was evaporated using a process of heating and

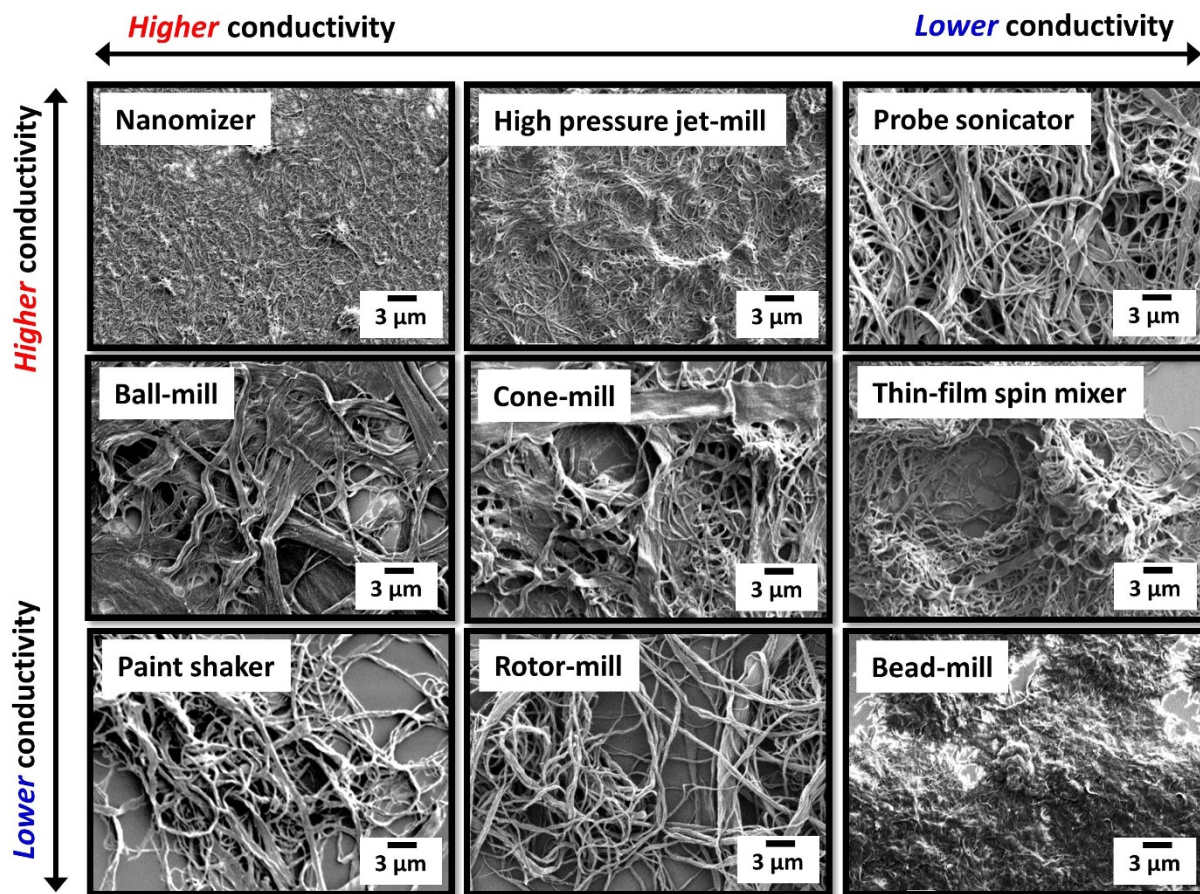


Figure 3 | SEM images of the structures of SG-SWCNT dispersions produced using different dispersion methods.

mechanical stirring, followed by vacuum drying at 80°C, to fabricate the composite sheets.

We found that the electrical conductivity of composites as measured using the four-probe method varied by a factor of ~ 4 among the different dispersion methods, as shown in Fig. 2a. The highest conductivity (~ 33 S/cm) was observed for dispersion using the Nanomizer, followed by high-pressure jet milling (~ 30 S/cm), while rotor milling and bead milling yielded the lowest conductivity (< 8 S/cm). Generally, when CNTs are added as a filler in composites, the electrical conductivity changes dramatically on a log scale in the region near the percolation threshold. After this region of drastic increase, however, the rate of increase in the conductivity drops, and the addition of more filler will not enhance the conductivity to any significant degree. For SG-SWCNTs, this percolation threshold is ~ 0.05 wt%. Near the percolation region (0.1 wt%), a change in conductivity of one order of magnitude can result from the use of a different CNT dispersion method (see Supplementary Table S1 online). Here, all of our conductivity results are achieved above this percolation threshold and thus represent values in the saturation regime (10 wt%). We believe that the factor of ~ 4 difference in conductivity makes a big difference, since the amount of CNT loading can be reduced by ~ 4 times, which has a huge impact on practical applications.

To address the generality of the dependence of the composite performance on the dispersion method, we prepared a different type of composite and repeated the investigation. Instead of a rubber composite, we dispersed the SG-SWCNTs in polystyrene (PS), a representative polymer matrix used in protective packaging, the manufacturing of appliances, household goods, and construction applications. As shown in Fig. 2b, the electrical conductivity of the PS composites showed a trend almost identical to that of the rubber

composite, and a conductivity range spanning a factor of ~ 3 was again observed. The Nanomizer and high-pressure jet milling again produced the highest conductivity, while rotor milling and bead milling produced the lowest conductivity. In addition, the composite mechanical properties were investigated using tensile test as shown in Supplementary Fig. S1. The mechanical properties of composites prepared using the Nanomizer and high-pressure jet milling showed the highest tensile strength (~ 4 times that of bead milling, ~ 2 times that of thin-film spin mixing) (see Supplementary Fig. S1 online). By comparing the different dispersion mechanisms, we find that the turbulent flow provides the highest electrical conductivity and mechanical property, followed by cavitation and then mechanical force. This demonstrates the importance of the dispersion mechanism in achieving high performance composites.

We repeated these experiments with six dispersion methods for three types of commercial MWCNTs including CNano (11 nm diameter, 10 μm length, $>95\%$ carbon purity), Nanocyl (9.5 nm diameter, 1.5 μm length, $>90\%$ carbon purity), and Baytubes (13 nm diameter, 1 μm length, $>95\%$ carbon purity). These three representative MWCNTs are shorter in length than the SG-SWCNTs. Besides the carbon purity which was provided by each of the makers, we performed additional thermal gravimetric analysis (TGA) of each of the CNTs to characterize the level of amorphous impurities. Generally, the TGA results indicate that CNano, Nanocyl and Baytubes possessed a relatively low level of amorphous carbon impurities, as the profiles do not drop more than 5% at temperatures $\sim 500^\circ\text{C}$. In contrast, the SG-SWCNTs and HiPco showed $\sim 10\%$ drop in weight at relatively low temperatures which would indicate $\sim 10\%$ level of amorphous content. However, the peak burning temperatures was found to be highest for the SG-SWCNTs and lowest for the HiPco SWCNTs, with the MWCNTs between. This result alone

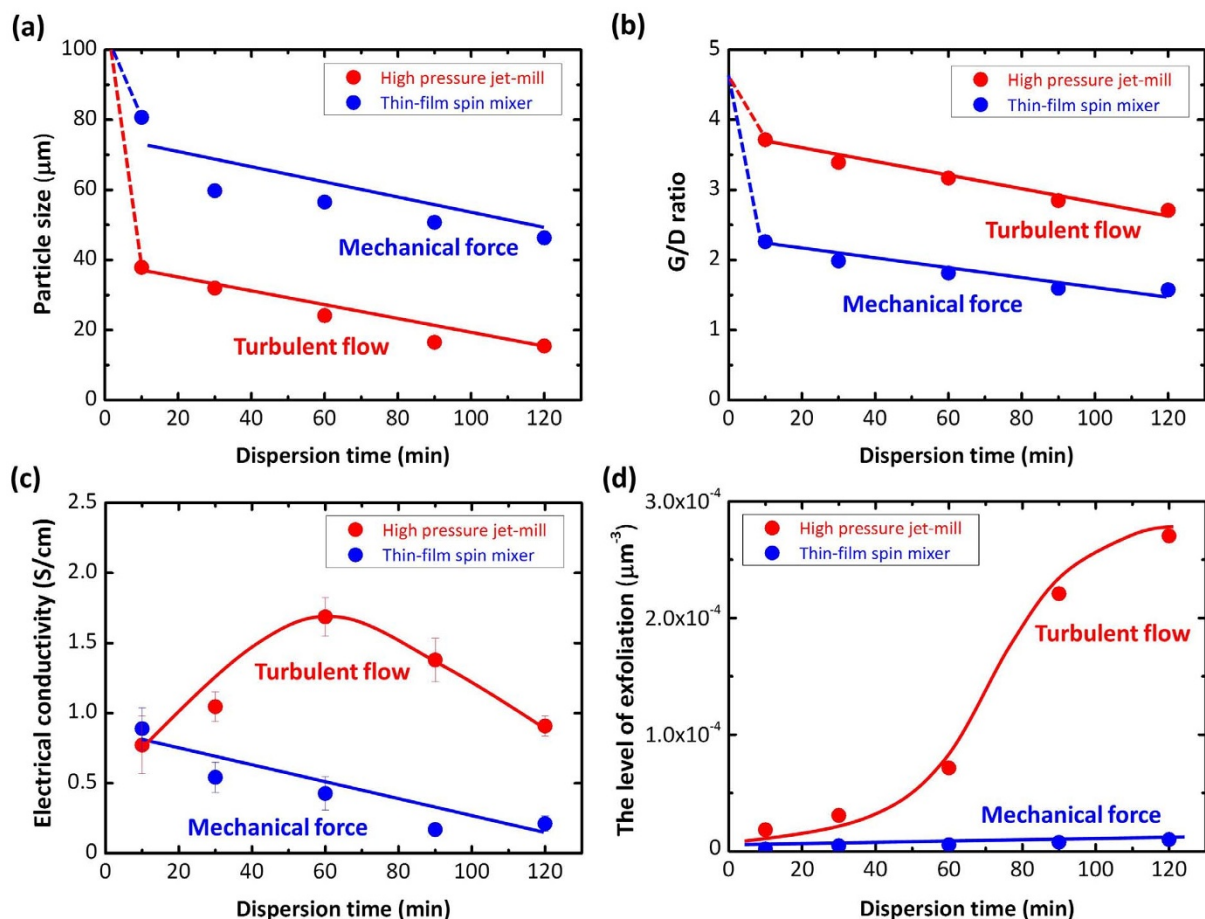


Figure 4 | Advantages of the turbulent flow dispersion method for producing advanced SG-SWCNT composites. SG-SWCNTs dispersed using high-pressure jet milling (100–120 MPa, 2 passes) as a turbulent flow method and thin-film spin mixing (30 m/s) as a mechanical force method for 10, 30, 60, 90, and 120 min. (a) Particle size and (b) G/D ratio of SG-SWCNTs dispersed for different times. (c) Electrical conductivity of 1 wt% SG-SWCNT/fluorinated rubber composites. (d) Level of exfoliation of SG-SWCNTs with increasing dispersion time.

is unclear, but likely is a result of the strong edge effects of the CNTs, i.e. short tubes (CNano, Nanocyl, Baytubes and HiPco) have many exposed edges than longer tubes (SG-SWCNTs). We can glean several important points by plotting the electrical conductivity of rubber composites made from MWCNTs as a function of the dispersion method (Fig. 2c). First, regardless of the dispersion method, the conductivities of SG-SWCNT/rubber composites were always higher. In particular, when the Nanomizer was used, the conductivity was more than 4 times higher for the SG-SWCNT/rubber composites. This result shows that long SWCNTs are superior to short MWCNTs for advanced composites. Second, in contrast to SG-SWCNTs, which showed a difference in electrical conductivity depending on the dispersion method, the MWCNTs did not show any noticeable difference for different dispersion methods. This result indicates that MWCNTs are insensitive to the dispersion method, while the dispersion method must be carefully chosen to extract the full potential of the SG-SWCNTs.

In order to understand why the electrical conductivity differed among the dispersion methods, we investigated the dispersion state of the SG-SWCNTs. Since the SG-SWCNT dispersion in the solution cannot be observed directly, we spin-coated the dispersion solution onto a substrate, dried it, and observed it using scanning electron microscopy (SEM). As shown in Fig. 3, we can see a significant difference between the dispersion states of the SG-SWCNTs. Dispersion by the Nanomizer and high-pressure jet mill produced a well-dispersed, uniformly fine mesh structure. We infer that the fine mesh structure was produced by exfoliation of the pristine CNTs

caused by the turbulent flow. Previous studies have shown that this mesh structure is a unique formation that appears only when long SWCNTs are dispersed¹⁶. This structure resembles the vein patterns observed in nature and is advantageous for transferring signals over large distances in arbitrary directions. Even without the use of surfactants, the fine mesh structure causes the suspension to have a shelf life of over a year because of the very large interfacial area between the SG-SWCNTs and the solution. The SG-SWCNTs can be stably suspended up to 3 wt%. When these SG-SWCNT mesh structures are incorporated into polymer matrices, the resulting composite has higher electrical conductivity. On the other hand, dispersion using methods based on mechanical force produced huge aggregated bundles that were roughly entangled. We believe that the lower conductivity of these composites is a direct result of the non-uniformly dispersed SG-SWCNTs. Dispersion by bead milling, which yielded the lowest conductivity, did not produce a well-dispersed or fine mesh structure and resulted in ball-like clustering of the SWCNTs, which indicates CNT scission. This is similar to the dispersion structures observed for short CNTs, which means that the long SWCNTs have lost their advantage^{27–29}. The probe sonicator, which produced an intermediate level of conductivity, yielded a long assembly of bundles intermediate between the fine mesh and large bundles. To investigate the dispersion morphology of the samples in more detail, transmission electron microscopy (TEM) and Raman spectroscopy characterization were performed for all dispersion methods (see Supplementary Fig. S2 online). TEM characterization indicated that the Nanomizer and high-pressure jet milled CNT dispersions showed

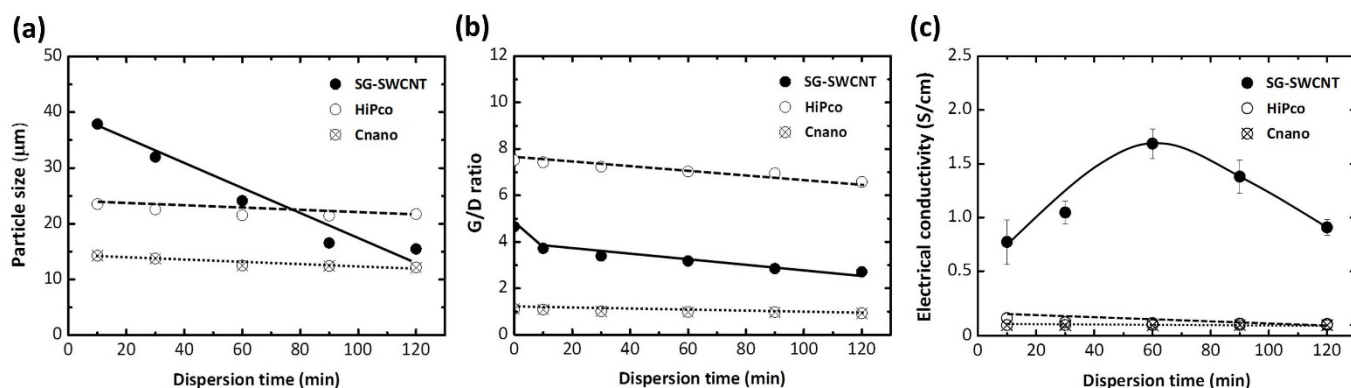


Figure 5 | Effect of the turbulent flow dispersion method (high-pressure jet milling, 100–120 MPa, 2 passes) on the different types of CNTs (HiPco and Cnano). Comparison of the CNT dispersion structure and properties of composites: (a) Particle size and (b) G/D ratio of SG-SWCNTs dispersed for different times. (c) Electrical conductivity of 1 wt% CNT/fluorinated rubber composites.

the highest level of debundling. Other methods showed very thick and unbundled aggregates of CNTs. The G/D ratio (intensity ratio of the G-band to the D-band) of pristine SG-SWCNTs was ~ 4.7 . The Nanomizer and high-pressure jet mill methods were among the methods to exhibit the highest G/D ratios along with cone milling, ball milling, and high shear batch disperser. Combining this data with the TEM image, it is clear that Nanomizer and high-pressure jet mill methods showed the best ability to create a debundled and far-encompassing network structure while inducing minimal damage to the CNTs. By plotting the electrical conductivity data versus the Raman data, higher G/D ratios clearly showed higher electrical conductivities of composite (see Supplementary Fig. S3 online). From these results, we can conclude that a homogenous dispersion of SWCNTs forming a long-range fine mesh with a minimum of scission is ideal for enhanced electrical conductivity of composites.

Discussion

To explore the correlation between the different dispersion mechanisms and the resultant dispersion state, we illustrated the process of SG-SWCNT dispersion by a turbulent flow and by mechanical force. As described above, dispersions based on turbulent flow produced composites with the highest conductivity, while composites made using mechanical force showed the lowest conductivity. The essential difference between these two mechanisms is that turbulent flow produces biaxial shearing forces, while mechanical force provides a shearing force only in a single direction. When long, aligned SWCNTs are exposed to solvents, capillary forces act to wick the CNTs into a big bundle. To disperse a SG-SWCNT forest, there must be a process to exert a counter effect that exfoliates the forest. Dispersion by biaxial shearing forces would be a significant advantage for exfoliation, since there would be a force acting to separate the aligned CNTs (see Fig. 2d). In contrast, when the long aligned CNTs exposed to uniaxial shearing forces during mechanical force dispersion, the exfoliation effect would be weak, since the CNTs will align in the direction of the force, and no force will act to pull the CNTs apart (see Fig. 2e). Instead, the CNTs would be squeezed and would collapse into huge bundles, as was experimentally observed in Fig. 3.

In order to gain deeper insight into the differences between the turbulent force and mechanical force dispersion mechanisms, we plotted various parameters in Fig. 4 as a function of process time, where high-pressure jet milling represents a turbulent flow method and thin-film spin mixing represents a mechanical force method. For each dispersion time, the resultant solution was characterized by performing laser diffraction (LD) to measure the size of the SWCNT aggregates (Fig. 4a) and obtaining the Raman spectra to determine the G/D ratio, which is an indicator of the damage to the CNTs induced by the dispersion (Fig. 4b). The initial size of the SG-

SWCNT forest flake was $\sim 650 \mu\text{m}$. The particle size as measured by LD showed a monotonic decrease with dispersion time for both methods. In addition, the particle sizes were significantly smaller for the turbulent flow than for the mechanical force. The particle size is an indicator of how well the SWCNTs have been dispersed, and in general, a smaller agglomerate shows higher performance. These results mean that with dispersion time, the SG-SWCNTs become increasingly homogeneous and enter a highly dispersed state for turbulent flow as compared to mechanical force. The initial G/D ratio was ~ 4.7 , and with dispersion time this value decreased gradually for both methods. The G/D ratio was significantly higher for the turbulent flow than for the mechanical force. The decrease in G/D ratio is due to the damage induced by the dispersion processes. Although the experimental results indicate that the damage increases with dispersion time, the turbulent flow produces less damage than the mechanical force. An interesting trend was observed when the electrical conductivity was plotted versus the dispersion time (Fig. 4c). For high-pressure jet milling, as the dispersion time increased, the conductivity of the 1 wt% SWCNT composite increased from $\sim 0.8 \text{ S/cm}$ up to $\sim 60 \text{ min}$, where it peaked at $\sim 1.7 \text{ S/cm}$, and with further dispersion the electrical conductivity began to drop. In contrast, the same composite made using thin-film spin mixing showed a monotonic drop from 0.8 to less than 0.2 S/cm over the same dispersion time range. It is important to note that for all dispersion times, the high-pressure jet milling yielded higher electrical conductivities than did thin-film spin mixing. The electrical conductivities were comparable for these two methods after $\sim 10 \text{ min}$ of dispersion, but the conductivity was ~ 4 times higher at its peak (60 min) for high-pressure jet milling, and still ~ 4 times higher even after it dropped (120 min).

The effect of the dispersion is an interplay between the level of exfoliation and the level of damage introduced to the CNTs, both of which increase with dispersion time. The former improves the performance, while the latter degrades it. Only when the advantage from exfoliation greatly outweighs the disadvantage due to damage can a high-performance composite be obtained. For a mechanical force method, regardless of the dispersion time, the loss due to damage appears to exceed the advantage of exfoliation. As a result, the performance of the composite simply decreases with dispersion time. This explains why for mechanical force dispersion, the best structures were the huge bundles, which reflect a very low level of exfoliation but also low damage. This essentially means that these methods cannot take full advantage of the long SWCNTs to fabricate a high-performance composite. For turbulent flow dispersion, the advantage of exfoliation was much higher, and the loss due to damage was much smaller. As a result, for short dispersion times, the composite performance increased. Once a fine mesh structure is obtained, the



advantage gained by further exfoliation greatly decreases while the damage monotonically increases, and thus the composite performance begins to degrade with further dispersion time.

We propose to quantify the degree of exfoliation as the cubic inverse of the particle size measured using LD. This parameter was chosen because the particle volume is expected to decrease with greater exfoliation, and therefore, to first-order, the two quantities will be inversely related. We plotted the level of exfoliation as a function of dispersion time for both the turbulent flow and mechanical force dispersion methods, which revealed several interesting features (Fig. 4d). The level of exfoliation for turbulent flow followed a sigmoid shape, in which the rate of exfoliation rapidly increased after 40 min. Here, we infer that the advantage from the exfoliation greatly exceeds the disadvantage from damage. However, after ~80 min the rate of exfoliation decreases and the level of exfoliation saturates at ~100 min. Therefore, we infer that here the disadvantage due to damage will overcome the advantage of exfoliation. When these effects are combined, we can expect to observe a peak between 40 and 80 min, which is in agreement with our experimental results. On the other hand, the exfoliation achieved by the mechanical force was much lower and did not increase dramatically as it did for turbulent flow, but instead increased linearly within this time range. This is the reason why the electrical conductivity did not exhibit a peak.

We further studied whether this exfoliation-damage dispersion mechanism, which is unique to the turbulent dispersion method, held true for other types of CNTs. We chose HiPco (0.8–1.2 nm diameter, 100–1,000 μm length, >80% carbon purity) to represent short SWCNTs and CNano to represent MWCNTs, but both were much shorter than the SG-SWCNTs. The pristine HiPco and CNano were supplied as heavily bundled, powdered agglomerates. As shown in Fig. 5, we repeated the experiments using the turbulent flow dispersion method (high-pressure jet milling), to characterize resultant solutions using LD and Raman spectroscopy after different dispersion times and then made the composites and measured their electrical conductivities. First, for HiPco and CNano, the particle size decreased only slightly with dispersion time (Fig. 5a). This suggests that exfoliation was ineffective for the short tubes. In contrast to CNano, whose G/D ratio essentially remained constant and low, HiPco and SG-SWCNTs both showed monotonic decreases in their G/D ratios (Fig. 5b). The electrical conductivities of the composites made with 1 wt% HiPco and CNano were much lower than that obtained with SG-SWCNTs (Fig. 5c), which again demonstrates that long SWCNTs were superior fillers. We believe that the ineffective exfoliation for the HiPco and CNano CNTs led to their inferior composite properties.

In conclusion, we have established a strategy for long SWCNT dispersion and an understanding of the dispersion mechanism, which will help in exploiting the full potential of long SWCNTs for use in high-performance composites. We found that when long SWCNTs were dispersed using a turbulent flow method, the resulting composites showed the highest performance compared to 1) composites with other types of CNTs (CNano, Nanocyl, Baytubes, and HiPco), 2) composites prepared using other dispersion methods. We propose a fundamental mechanism to explain this unique effect, namely, that turbulent flow provides much higher level of exfoliation than other methods, which is only observed when long SWCNTs are used. Only when exfoliation overcomes the disadvantage due to damage can a high-performance composite be made. We envision that this fundamental understanding regarding the dispersion of long SWCNTs will serve as a guide for future research on extracting the full potential of the pristine SWCNT material in CNT composites and thus will eventually open up many new opportunities.

Methods

SG-SWCNT synthesis. SG-SWCNTs were synthesized in a fully automatic 100-tube furnace using water-assisted chemical vapor deposition with a C₂H₄ carbon source on Fe–Ni–Cr alloy metal foils with Fe/Al₂O₃ catalyst metal films. He and H₂ were used as

the carrier gases (total flow rate = 1,000 sccm) at 1 atm with a controlled amount of water vapor (concentration 100–150 ppm). Growth was carried out at 750 °C with C₂H₄ (100 sccm) for 10 min. The height of the synthesized SG-SWCNT forest was from 100 μm up to 1 mm.

Materials. Fluorinated rubber (Daiel-G912 from Daikin Industries, Ltd.) and polystyrene (HF77 from PS Japan Corporation) were used as the matrix materials. Three types of MWCNTs were used: CNano (FloTube 9000 from CNano Technology Ltd.), Nanocyl (NC 7000 from Nanocyl S.A.), and Baytubes (Baytubes C70P from Bayer AG). HiPco SWCNTs were obtained from Unidym Inc. The purity of CNTs used in this study was evaluated by using Thermogravimetry (Q5000, TA Instruments) (see Supplementary Fig. S4 online).

Preparation of CNT composites. CNT composites were prepared using solution casting. The CNTs were dissolved in methyl isobutyl ketone (MIBK) and dispersed under the optimized dispersion conditions using 11 different dispersion methods (methods involving the use of Nanomizer, high-pressure jet mill, probe sonicator, ball mill, bead mill, paint shaker, ball collision mill, cone mill, rotor mill, high-shear batch disperser, and thin-film spin mixer). The concentration of CNTs was 0.1 wt%. CNT-MIBK dispersions were mixed with fluorinated rubber or a PS solution to yield the 10 wt% and 1 wt% CNT composites. These solutions were homogenized by stirring at 80 °C and poured into a Petri dish for solvent removal. Then, each dish was dried in a vacuum oven at 80 °C. After drying, the CNT composites were obtained as sheets.

Measurement of electrical and mechanical properties of CNT composites. The electrical conductivities of the composites were measured using a four-point probe method (MCP-T610, Mitsubishi Chemical Analytech Co., Ltd.). The tensile test was carried out using Autograph universal testing system (AG-IS, Shimadzu Corp.) with crosshead speed of 1 mm/min.

Characterization of the structure of the CNT dispersions. Scanning electron microscopy (SEM) (FE-SEM S-4800, Hitachi High-Technologies Co.) was performed to observe the dispersed CNT structures. The specimens for SEM were made by spin-coating the CNT-MIBK dispersions on Si substrates. Transmission electron microscopy (TEM) (EM-002B, TOPCON Corp.) was used to investigate the dispersion morphology in more detail. Sonication treatments are commonly used for preparing TEM specimens of CNTs. Since this step may lead to the structural changes of original CNT dispersion, we diluted the dispersion solution and dropped directly on TEM grids. Laser diffraction (LD) measurement was performed to estimate the sizes of the dispersed tubes or bundles using an LD analyzer (MT3300EX, NIKKISO Co., Ltd.). The CNT dispersions were diluted with MIBK before the measurements. Raman spectra of the CNT-MIBK dispersions, which were drop-cast onto glass-slides were obtained using a Raman spectrometer (Nicolet Almega XR, Thermo Fisher Scientific Inc.) with laser excitation at a wavelength of 532 nm.

- Ajayan, P. M., Stephan, O., Colliex, C. & Trauth, D. Aligned carbon nanotube arrays formed by cutting a polymer resin-nanotube composite. *Science* **265**, 1212–1214 (1994).
- Baughman, R. H., Zakhidov, A. A. & de Heer, W. A. Carbon nanotubes—the route toward applications. *Science* **297**, 787–792 (2002).
- McCarthy, B. *et al.* A microscopic and spectroscopic study of interactions between carbon nanotubes and a conjugated polymer. *J. Phys. Chem. B* **106**, 2210–2216 (2002).
- Breuer, O. & Sundararaj, U. Big returns from small fibers: a review of polymer/carbon nanotube composites. *Polym. Compos.* **25**, 630–645 (2004).
- Thostenson, E. T., Li, C. & Chou, T. W. Nanocomposites in context. *Compos. Sci. Technol.* **65**, 491–516 (2005).
- Byrne, M. T. & Gun'ko, Y. K. Recent advances in research on carbon nanotube-polymer composites. *Adv. Mater.* **22**, 1672–1688 (2010).
- Grady, B. P. Recent developments concerning the dispersion of carbon nanotubes in polymers. *Macromol. Rapid Commun.* **31**, 247–257 (2010).
- Du, J. H., Bai, J. & Cheng, H. M. The present status and key problems of carbon nanotube based polymer composites. *Express Polym. Lett.* **1**, 253–273 (2007).
- Zheng, L. X. *et al.* Ultralong single-wall carbon nanotubes. *Nat. Mater.* **3**, 673–676 (2004).
- Kim, H. *et al.* Synthesis of ultra-long super-aligned double-walled carbon nanotube forests. *J. Nanosci. Nanotechnol.* **11**, 470–473 (2011).
- Li, X. *et al.* Air-assisted growth of ultra-long carbon nanotube bundles. *Nanotechnol.* **19**, 455609–15 (2008).
- Hata, K. *et al.* Water-assisted highly efficient synthesis of impurity-free single-walled carbon nanotubes. *Science* **19**, 1362–1364 (2004).
- Yasuda, S. *et al.* Improved and large area single-walled carbon nanotube forest growth by controlling the gas flow direction. *ACS Nano* **3**, 4164–4170 (2009).
- Yasuda, S., Futaba, D. N., Yamada, T., Yumura, M. & Hata, K. Gas dwell time control for rapid and long lifetime growth of single-walled carbon nanotube forests. *Nano Lett.* **11**, 3617–3623 (2011).
- Ata, S., Kobashi, K., Yumura, M. & Hata, K. Mechanically durable and highly conductive elastomeric composites from long single-walled carbon nanotubes mimicking the chain structure of polymers. *Nano Lett.* **12**, 2710–2716 (2012).



16. Subramaniam, C. *et al.* One hundred fold increase in current carrying capacity in a carbon nanotube–copper composite. *Nat. Commun.* **4**, 2202 (2013).
17. Ma, P. C., Siddiqui, N. A., Marom, G. & Kim, J. K. Dispersion and functionalization of carbon nanotubes for polymer-based nanocomposites: a review. *Compos. Part A*. **41**, 1345–1367 (2010).
18. Hilding, J., Grulke, E. A., Zhang, Z. G. & Lockwood, F. Dispersion of carbon nanotubes in liquids. *J. Disper. Sci. Technol.* **24**, 1–41 (2003).
19. Xu, G. H. *et al.* A two-step shearing strategy to disperse long carbon nanotubes from vertically aligned multiwalled carbon nanotube arrays for transparent conductive films. *Langmuir* **26**, 2798–2804 (2010).
20. Lu, K. L. *et al.* Mechanical damage of carbon nanotubes by ultrasound. *Carbon* **34**, 814–816 (1996).
21. Cotiuga, I. *et al.* Block-copolymer-assisted solubilization of carbon nanotubes and exfoliation monitoring through viscosity. *Macromol. Rapid Commun.* **27**, 1073–1078 (2006).
22. Mukhopadhyay, K., Dwivedi, C. D. & Mathur, G. N. Conversion of carbon nanotubes to carbon nanofibers by sonication. *Carbon* **40**, 1373–1376 (2002).
23. Sekitani, T. *et al.* Stretchable active-matrix organic light-emitting diode display using printable elastic conductors. *Nat. Mater.* **8**, 494–499 (2009).
24. Sekitani, T. *et al.* A rubberlike stretchable active matrix using elastic conductors. *Science* **321**, 1468–1472 (2008).
25. Tsuchiya, K. *et al.* High electrical performance of carbon nanotubes/rubber composites with low percolation threshold prepared with a rotation–revolution mixing technique. *Compos. Sci. Tech.* **71**, 1098–1104 (2011).
26. Kobashi, K. *et al.* A dispersion strategy: dendritic carbon nanotube network dispersion for advanced composites. *Chem. Sci.* **4**, 727–733 (2013).
27. Inam, F., Reece, M. J. & Peijs, T. Shortened carbon nanotubes and their influence on the electrical properties of polymer nanocomposites. *J. Compos. Mater.* **46**, 1313–1322 (2011).
28. Xu, H. *et al.* Efficient dispersing and shortening of super-growth carbon nanotubes by ultrasonic treatment with ceramic balls and surfactants. *Adv. Powder Technol.* **21**, 551–555 (2010).
29. Simien, D. *et al.* Influence of nanotube length on the optical and conductivity properties of thin single-wall carbon nanotube networks. *ACS Nano* **2**, 1879–1884 (2008).

Acknowledgments

Support by the New Energy and Industrial Technology Development Organization is acknowledged. We would like to thank Mr. T. Mizuno and N. Yahata for helpful assistance.

Author contributions

H.Y., M.Y. and S.A. designed the experiments and discussed the results. H.W. and M.Y. conducted the experiments and collected all data. D.F. and T.Y. discussed the results and helped in drafting the manuscript. K.H. supervised the overall research and conceived the initial idea of the experiments. All authors read and commented on the manuscript.

Additional information

Supplementary information accompanies this paper at <http://www.nature.com/scientificreports>

Competing financial interests: The authors declare no competing financial interests.

How to cite this article: Yoon, H. *et al.* Controlling exfoliation in order to minimize damage during dispersion of long SWCNTs for advanced composites. *Sci. Rep.* **4**, 3907; DOI:10.1038/srep03907 (2014).



This work is licensed under a Creative Commons Attribution-NonCommercial-NoDerivs 3.0 Unported license. To view a copy of this license, visit <http://creativecommons.org/licenses/by-nc-nd/3.0>